Article

The Modification of WO₃ for Lithium Batteries with Nickel-Rich Ternary Cathode Materials

Lipeng Xu [1,*] , **Chunjiang Bao** [1] , **Haobing Zhou** [2] **and Jun Li** [3]

1 School of Mechanical and Automotive Engineering, Liaocheng University, Liaocheng 252000, China; baochunjiang@lcu.edu.cn
2 School of Mechatronics Engineering, Zhongyuan University of Technology, Zhengzhou 450007, China; haobingzhou@zut.edu.cn
3 School of Aviation and Transportation, Jiangsu College of Engineering and Technology, Nantong 226007, China; lijun7239@nuaa.edu.cn
* Correspondence: xulipeng@lcu.edu.cn; Tel.: +86-18263533137

Abstract: Nickel-rich ternary cathode materials (NRTCMs) have high energy density and a long cycle life, making them one of the cathode materials of LIB that are currently receiving much attention. However, it has shortcomings such as poor cycling performance (CP) and a high-capacity decay rate. Because of this, the study analyzed the modification effect of WO_3 on NRTCM lithium batteries by preparing WO_3-modified poly-crystal and single-crystal NCM622 materials under the existing conditions of better original cathode materials as reference samples. The results showed that in the morphology and structure testing, with the increase of WO_3 addition, the c/a values of all NCM622-WO_3 samples were greater than 4.95. In the analysis of cycling and rate performance (CRP), as W increased, the rate performance (RP) of the NCM622-W4.0 sample had a discharge specific capacity ratio of 86.2% at 10.0 C/1.0 C. In cyclic voltammetry testing, when the addition amount of WO_3 was 1.0%, the polarization degree of SC-NCM622 sample was the weakest. In the AC impedance test, after six cycles, compared with the original sample, the Ret and R + Rct values of the NCM622-W sample modified with WO_3 showed a significant downward trend. The above results prove that WO_3 modification can lower the polarization of the material, effectively raising the CRP of the battery. It provides a reference path for the further progress of high capacity and stability ternary cathode materials.

Keywords: lithium battery; nickel rich ternary cathode materials; tungsten trioxide; modification; preparation

1. Introduction

Energy is a powerful driving force for the progress and development of human society, and the series of natural disasters caused by greenhouse gases caused by energy consumption have posed a serious threat to human survival. Developing a green industrial revolution and utilizing clean and renewable energy to achieve carbon substitution have become the only way to address this issue [1]. Renewable energy has the characteristics of discontinuity and low stability, requiring certain energy storage devices for storage [2]. With the continuous progress of technology, as a low-cost energy storage device, batteries have been continuously improved, and lithium-ion batteries stand out in this process. Compared with traditional secondary batteries, lithium-ion batteries have small self-discharge and no memory effect and are widely used in electric vehicles and other fields [3]. With the continuous improvement of the economic level, the demand for new energy vehicles by the public is increasing day by day [4]. It is necessary to promote the application of large-scale energy storage power stations and electric vehicles and develop lithium-ion batteries with a longer cycle life and higher energy density. The positive electrode material is a crucial component in lithium-ion batteries, which directly affects the energy density, lifespan,

and other aspects of the battery [5]. In recent years, various positive electrode materials have constantly caught people's attention, accompanied by various problems, making it difficult to meet people's demand for low-cost and high-performance lithium-ion batteries. WO_3-modified material is a material that has been studied for its potential use in lithium electronic batteries. WO_3, with a high theoretical ability and stability, is one of the key points to become the cathode material in lithium-ion batteries. WO_3, a transition metal semiconductor with a band gap of about 2.6 eV, is an important functional material due to its superior physical and chemical properties. At present, WO_3-modified materials have been widely used in the preparation of lithium-ion batteries. Lithium-ion batteries are widely used in a variety of portable electronic products, electric vehicles, and energy storage systems, and many scholars are actively looking for new materials for synthesis to improve their performance [6].

With the development and application of positive electrode materials, more and more scholars are starting to study different preparation materials [7]. Xiao Z and Liu P et al. analyzed the structure and structural defects of nickel-rich ternary cathode materials. During the process, effective strategies to improve the performance of hot spots were summarized, such as the changes in material structure after improving battery performance, as well as the mechanisms of element doping and surface coating changes. It was finally found that the key to improve the safety of lithium batteries was the structural stability of nickel-rich ternary cathode materials [8]. Lee G and other researchers have developed a functionalized nickel-rich lithium metal oxide cathode material by utilizing a heat treatment process design and combining various uses of nano-inorganic materials such as titanium silicon oxide. The experiment found that after 100 cycles, the dissolution of transition metals can effectively inhibit the decomposition of electrolytes. The conclusion proves that using nano-titanium silicate to produce the coatings of nickel-rich lithium metal oxide cathode materials can significantly improve the cycling performance of lithium batteries [9]. Mao G's team proposed preparing a new type of dual coating material and cathode material for lithium batteries using isopropoxyaluminum ($C_9H_{21}AlO_3$) and isopropyl titanate ($C_{12}H_{28}O_4Ti$) through hydrolysis and lithiation processes. The microscopic characterization results show that the proposed structure can effectively suppress side reactions, changes in structure, and cracks at the cathode or electrolyte interface and ultimately significantly improve the chemical performance of lithium batteries [10]. Scholars such as Xia D proposed using synthesized submicron single crystals to prepare cathode materials for lithium batteries, in order to improve the stability of the materials and the cycling performance of lithium batteries. The results show that because of its unique morphology and stable structure, the single crystal can effectively reduce the surface cracks, polarization, and side reactions of the cathode material and thus effectively improve the rate performance of the battery [11]. Geng Z and Shi W et al. proposed using solid-state PEO-LLZTO as an electrolyte for experiments in order to suppress the outflow of active materials and effectively improve the cycling performance of electrode materials. During the process, the weights of PEO molecules and different electrolyte additives were adjusted to ultimately determine the preparation of material capacity [12]. Kaneda H et al. proposed mixing Ni with AL to prepare a new lithium-ion battery material. After cycling the lithium battery prepared by the material 500 times in the entire battery, the mixed $LiNi_xAl_{1-x}O_2$ material which showed excellent capacity retention. The results show that $LiNi_xAl_{1-x}O_2$ synthesized under optimal conditions is a promising electrode material with no reason for nickel enrichment (Ni $\geq$ 80 at%) [13]. Cx A et al. used two different solvents as basic materials and prepared $CrNb_{49}O_{124}$ nanowires of different sizes through electrospinning technology. During the process, the obtained nanowires were nitrided with hot ammonia gas, resulting in a Coulombic efficiency of up to 90.72%. Simultaneously, it has excellent long cycle stability. The final results show that the electrochemical performance of the nanowire is significantly superior to most anode materials, making it an effective electrode material [14].

Based on the above, it can be concluded that nickel-rich ternary material (NCM) is one of the few positive electrode materials for batteries that can meet the requirements of high

density. However, under high current density, its capacity decay rate is too high, and its cycling performance is poor. At the same time, this material is prone to grain boundary cracking, leading to the collapse of the material structure and reducing its dynamic performance. In addition, the discharge-specific capacity of a single crystal is relatively low, and the magnification performance is poor, which hinders the application and promotion of high-power electric vehicles [15,16]. Therefore, in order to improve the poor cycling stability of the reference material, based on the temperature of preparing nickel-rich ternary material NCM811, a commercial nickel rich ternary material 622 precursor with better particle morphology and electrochemical performance was selected as the research object. Under the existing conditions of better original cathode material as the reference material, the influence of WO_3 on the morphology, structure, and electrochemical performance of NCM622 and single-crystal ternary material (SC-NCM622) was explored, and comprehensive analysis to further improve the electrochemical performance of electrode materials was conducted.

2. The Modification of WO_3 for Lithium Batteries with NRTCMs

2.1. Experimental Materials, Instruments, and Characterization Testing

2.1.1. Experimental Materials

With high energy and power density and a long cycle life, LIBs have been successfully commercialized. To analyze the performance of ternary cathode materials for synthetic lithium batteries, suitable chemical reagents were selected for the experiment. The chemical reagents required for the experiment are shown in Table 1 [17,18].

Table 1. Main Chemical Reagents Required for the Experiment.

Reagent Name	Chemical Formula	Specifications	Manufacturer
Lithium Hydroxide MonoHydrate	$LiOH \cdot H_2O$	≥98%	Hangzhou, China, Aladdin Company
Lithium carbonate	Li_2CO_3	>98%	Hangzhou, China, Aladdin Company
Nickel sulfate hexahydrate	$NiSO_4 \cdot 6H2O$	≥99%	Hangzhou, China, Aladdin Company
Cobalt sulfate heptahydrate	$CoSO_4 \cdot 7H_2O$	≥99%	Hangzhou, China, Aladdin Company
Manganese sulfate monohydrate	$MnSO_4 \cdot H_2O$	≥99%	Hangzhou, China, Aladdin Company
Acetylene black	C	Battery level	Shenzhen, China, Xilong Chemical Co., Ltd.
N-methylpyrrolidone	C_5H_9NO	Battery level	Hangzhou, China, Aladdin Company
ammonia	NH_4OH	25–28%	Hangzhou, China, Aladdin Company
Tungsten trioxide	WO_3	≥99%	Hangzhou, China, Aladdin Company
Vinylidene fluoride	$<(CH_2-CF_2)_n$-	Battery level	Shenzhen, China, Xilong Chemical Co., Ltd.
electrolyte	$LiPF_6(EC:EMC:DMC)$	Battery level	Suzhou, China, Duoduo Chemical Reagent Network
Lithium flake	Li	Battery level	Suzhou, China, Duoduo Chemical Reagent Network
the diaphragm	PP/PE/PP	Battery level	Shenzhen, China, Shenzhen Kejing Co., Ltd.
Battery case	--	Battery level	Taiyuan, China, Shanxi Lizhiyuan Battery Materials Co., Ltd.

2.1.2. Experimental Instruments and Equipment

With selecting the experimental materials required for the research, the main instruments for analyzing material properties are statistically analyzed. The main instruments and equipment required for the experiment are shown in Table 2.

Table 2. Main instruments and equipment required for the experiment.

Experimental Instruments	Model	Manufacturer
Electronic balance	AR64CN	Changzhou Aohaosi Instrument Co., Ltd., Changzhou, China
A magnetic stirrer	79-2	Leici Company, Shanghai, China
Ultrasonic cleaning machine	KQ3200DB	Kunshan Ultrasonic Instrument Company, Kunshan, China
Vacuum drying oven	DZF-6050	Changzhou Henglong Instrument Co., Ltd., Changzhou, China
Glove box	Lab 2000	Etelux Company, Beijing, China
Automatic coating machine	PX-TB-W1	Pengxiang Yunda Co., Ltd., Shenzhen, China
Experimental roller press	PX-GY-100	Pengxiang Yunda Co., Ltd., Shenzhen, China
Button cell hydraulic sealing machine	PX-YF-20	Pengxiang Yunda Co., Ltd., Shenzhen, China
Atmosphere tube electric furnace	SK-G05143	Tianjin Zhonghuan Electric Furnace Co., Ltd., Tianjin, China
Gamry Electrochemical Workstation	Reference 600	Gamry Instruments, Inc, Philadelphia, PA, USA
Scanning electron microscope	JSM-6510	Japan Corporation, Aichi Kariya City, Japan
Scanning electron microscope	Zeiss Sigma 500	Carl Zeiss (Shanghai) Management Co., Ltd., Oberkoheng, Germany
Transmission electron microscope	Tecnai G2 F20	FEI Corporation of the United States, Hillsboro, OR, United States
X-ray photoelectron spectrometer	Thermo ESCALAB 250XI	Thermo Fisher Scientific, Waltham, MA, USA
X-ray diffractometer	Mini Flex600	Nippon Science Corporation, Shanghai, China
Vacuum circulating water suction filter	SHZ-D(III)	Henan Yuhua Instrument Co., Ltd., Luoyang, China

2.1.3. Material Characterization Testing

There are two main types of research using scanning electron microscopy (SEM): JSM-6510 and Zeiss Sigma500. High resolution surface morphology observation of different samples using SEM can intuitively observe the surface morphology of the samples, such as their shape and size [19,20].

Transmission Electron Microscope (TEM) can be used to observe fine structures of materials smaller than 200 nm and to determine the microstructure of the material, including information such as lattice stripes and crystal plane spacing, using X-ray diffraction and scattering effects in crystalline and amorphous materials to achieve X-ray Powder Diffractometer (XRD) testing [21].

Information on the elements and valence states present in the material is obtained by X-ray photoelectron spectroscopy (XPS). In addition, the relative content of each valence state element in the material is determined by the spectral line area in the energy spectrum. The study obtained the Warburg coefficient through the fitting graph in the results and further calculated the lithium-ion diffusion coefficient $D_{Li}{}^+$ of all samples, as shown in Equation (1).

$$D_{Li}{}^+ = R^2 T^2 / \left(2A^2 n^4 F^2 C^2 \sigma^2 \right) \tag{1}$$

In Equation (1), R, T, A, n, F, C separately represent the gas constant, absolute temperature, electrode area, the number of electrons contained in each molecule in the LIB material, Faraday constant, and the number of lithium ions per identity element cell volume.

2.2. Basic Preparation of NRTCMs

One of the raw materials for the preparation of ternary materials is the ternary precursor, and the selection of raw materials greatly affects the preparation of ternary cathode materials. The difference in physical and chemical properties of ternary precursors directly affects the EP of nickel-rich ternary cathode materials (NRTCMs). The main factors that cause these differences in properties include environment, synthesis temperature, acidity and alkalinity, and stirring speed. To prepare NRTCMs with excellent performance, it is necessary to synthesize ternary precursors with good crystallinity and uniform particle size [22,23]. NCM811 was prepared by coprecipitation method. The flow chart is shown in Figure 1.
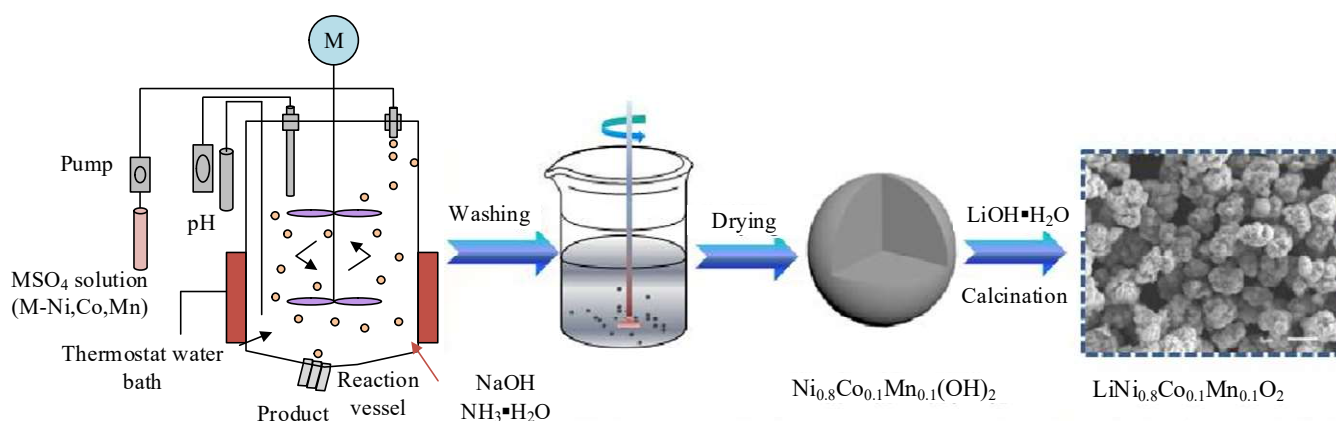

Figure 1. Schematic diagram of $LiNi_{0.8}Co_{0.1}Mn_{0.1}O_2$ prepared by a coprecipitation method.

In Figure 1, the preparation of ternary cathode materials by the coprecipitation method can be divided into six steps. The first step is to select sulfate as the raw material. It weighs $NiSO_4 \cdot 6H_2O$, $MnSO_4 \cdot H_2O$, and $CoSO_4 \cdot 7H_2O$ at a concentration of 2 mol/L, separately. The three liquids are mixed in a 400 mL mixed salt solution, stirred continuously for three hours to ensure that the sulfate in the solution is fully dissolved. In addition, it weighs 8 mol/L of NaOH and is prepared into 400 mL of alkaline solution. It needs to be continuously stirred for 3 h until it is completely dissolved. Finally, it uses a measuring cylinder to weigh 10 mol/L of NH3·HO, mixed with purified water to form a 400 mL solution, used as a complexing agent. The second step is to pour approximately 1.2 L of deionized water as the bottom solution into a glass reactor and heat the reactor in a water bath until the temperature rises to 50 °C. Nitrogen gas with a flow rate of 80 mL/min is introduced as a protective gas. The third step is to drop approximately 60 mL of ammonia water into the glass reactor, and by adjusting the amount of water dropped, the pH in the glass reactor is stabilized around 11.5. During the reaction, the amount of ammonia water dropped is dynamically adjusted to maintain the pH value of the entire reaction system at around 11.5. The stirring speeds of the experimental reaction are set to 900 rpm, 1000 rpm, and 1100 rpm, respectively. Subsequently, the material is fed at a rate of 2 mL/min, and the reaction officially proceeds. For Step 4, the total feeding lasts for about 5 h, and attention should be paid to the pH value, solution color, and ventilation conditions during the reaction. After the feeding is completed, there needs to be continuous stirring for 30 h until it has fully reacted. Subsequently, close the ventilation and stop stirring, and let the solution stand for 10 to 12 h to further grow the particles with a uniform particle size distribution. The fifth step is to extract the suspended solids in the reaction kettle and repeatedly clean the obtained $Ni_{0.8}Co_{0.1}Mn_{0.1}$ (OH) 2 precursor with deionized water. The precursor is put in a vacuum-drying oven and dried at 60 °C for 15 h. For Step 6, the molar ratio is set to 1:1.06, and it weighs the $Ni_{0.8}Co_{0.1}Mn_{0.1}$ (OH) 2 precursor and LiOH according to the molar ratio and continues stirring for 2 h. It places the mixed powder in a crucible and bakes it in stages in a high-temperature furnace. First, it is heated at 500 °C for 6 h and then at 800 °C for 15 h. Throughout the entire process, oxygen is used as the intermediate gas and

calcined at a temperature of 5 °C per minute. Finally, the melting is completed, and the required ternary cathode material is obtained [24,25].

2.3. The Modification of Polycrystalline NRTCMs by WO_3

The nickel-rich ternary material NCM exhibits excellent reversible specific capacity due to its high Ni content and is currently the most promising new type of cathode material for LIB. However, there are currently issues with poor cycling stability and rapid specific capacity decrease in NRTCMs. Meanwhile, the lower the Ni content of the ternary cathode material, the higher the temperature required for calcination. Research will use the calcination temperature of NCM811 as the basis and appropriately increase the calcination temperature. Before the experiment began, WO_3 was mixed evenly with polycrystalline NCM622 to obtain WO_3-modified polycrystalline NCM622 material. The preparation of WO_3 modified polycrystalline NCM622 material is shown in Figure 2.

$Ni_{0.6}Co_{0.2}Mn_{0.2}(OH)_2$

$LiCO_3$

WO_3

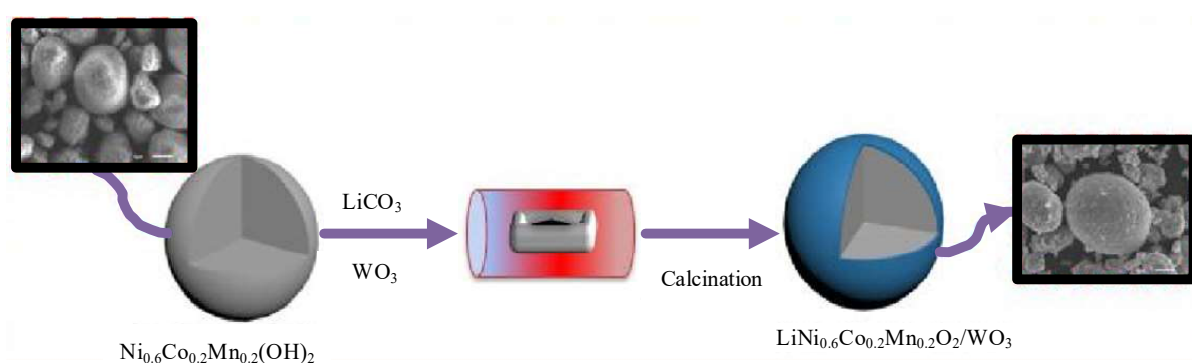Calcination

$LiNi_{0.6}Co_{0.2}Mn_{0.2}O_2/WO_3$

Figure 2. WO_3 schematic diagram of the preparation of the modified polycrystalline NCM622.

In Figure 2, the commercial polycrystalline precursor is weighed at a molar ratio of 1:1.06 and constantly ground for 3 h to achieve complete mixing. It places the ground raw materials into a crucible and calcines them in a high-temperature tube furnace. In an oxygen atmosphere, it sets the temperature to 500 °C for 6 h and then holds it at a high temperature of 920 °C for 15 h, maintaining a heating rate of 5 °C/min. After the reaction is completed, it lets the high-temperature furnace stand until the sample cools to room temperature, and polycrystalline NCM622 can be obtained, named NCM622-W0 [26,27]. The calcination conditions of the modified sample are the same as those of the NCM622-W0 sample, with the difference being that the WO_3, polycrystalline precursor, and LiCO3 materials are thoroughly mixed before calcination. The molar ratio of polycrystalline precursor to Li_2CO_3 is 1:1.06, and the mass percentages of WO_3 and polycrystalline precursor added are 0.5%, 1.0%, 1.5%, 2.0%, 2.0%, 2.5%, 3.2%, 4.0%, 5.0%, and 6.0%, respectively. According to the difference in the amount of WO_3 added, the modified samples are named NCM622-W0.5, NCM622-W1.0, NCM622-W1.5, NCM622-W2.0, NCM622-W2.5, NCM622-W3.2, NCM622-W4.0, NCM622-W5.0, and NCM622-W6.0, respectively.

2.4. The Modification of Single-Crystal NRTCMs by WO_3

Because of their high energy and power density, NRTCMs have become the main development direction for LIB. Nevertheless, batteries based on NRTCMs are prone to safety hazards such as "self ignition", which makes NRTCMs highly controversial in the market. At present, the research of NCM mainly focuses on structural stability, compactness, and cycle stability. Single-crystal nickel-rich cathode material (SC-NCM) is expected to become mainstream in the future, thus promoting the large-scale application of NRTCMs in new energy. The preparation schematic diagram of SC-NCM622 is shown in Figure 3.
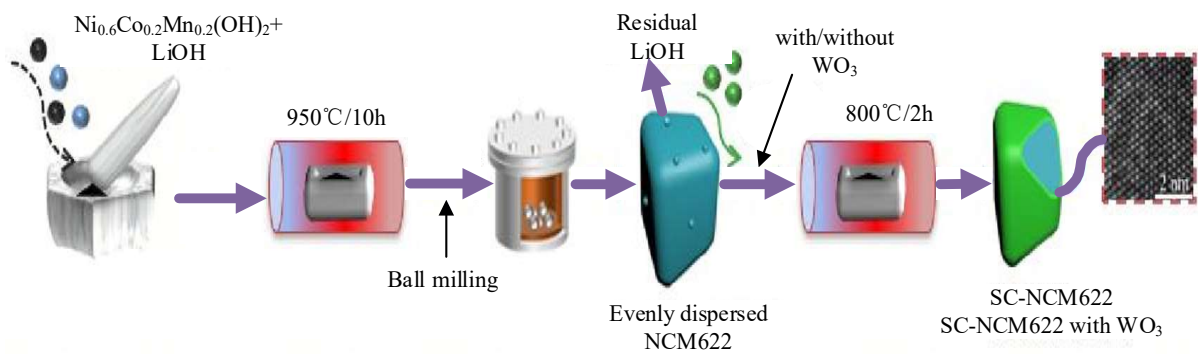
Figure 3. Schematic preparation of SC-NCM622.

In Figure 3, the specific operation can be divided into four steps. The first step is to weigh the commercial ternary cathode material precursor $Ni_{0.6}Co_{0.2}Mn_{0.2}$ (OH) 2 and LiOH in a molar ratio of 1:1.06 and continue grinding for 2 h to achieve complete mixing. The second step is to put the ground raw material into a crucible and calcine it for 10 h in a high-temperature tube furnace at 950 °C. Under oxygen atmosphere, it maintains a heating rate of 5 °C/min, and after the reaction, it obtains a ternary cathode material $LiNi_{0.6}Co_{0.2}Mn_{0.2}O_2$ (NCM622). The third step is to place NCM622 in a ball mill with a ball to material ratio of 10:1 and continue milling at a rate of 200 r/min for 1 h to get dispersed and granular NCM622 [28,29]. The fourth step is to place the granular NCM622 in a tubular furnace, and under an argon atmosphere, it raises the temperature of NCM622 to 800 °C at a rate of 5 °C/min and continues to calcine it for 2 h to obtain the original sample SC-NCM622. The mass ratios of NCM622 and WO_3 dispersed with mixed particles are 0.5%, 10%, and 1.5%, respectively. The SC-NCM622 modified with WO_3 obtained under the same calcination conditions are named SC-NCM622-0.5% WO_3, SC-NCM622-1.0% WO_3, and SC-NCM622-1.5% WO_3, respectively.

3. Result Analysis

3.1. Morphology and Structural Analysis

To investigate the outcome of WO_3 modification on the phase structure of single-crystal and poly-crystal NCM622, XRD tests were conducted on the samples before and after modification, as shown in Figure 4.
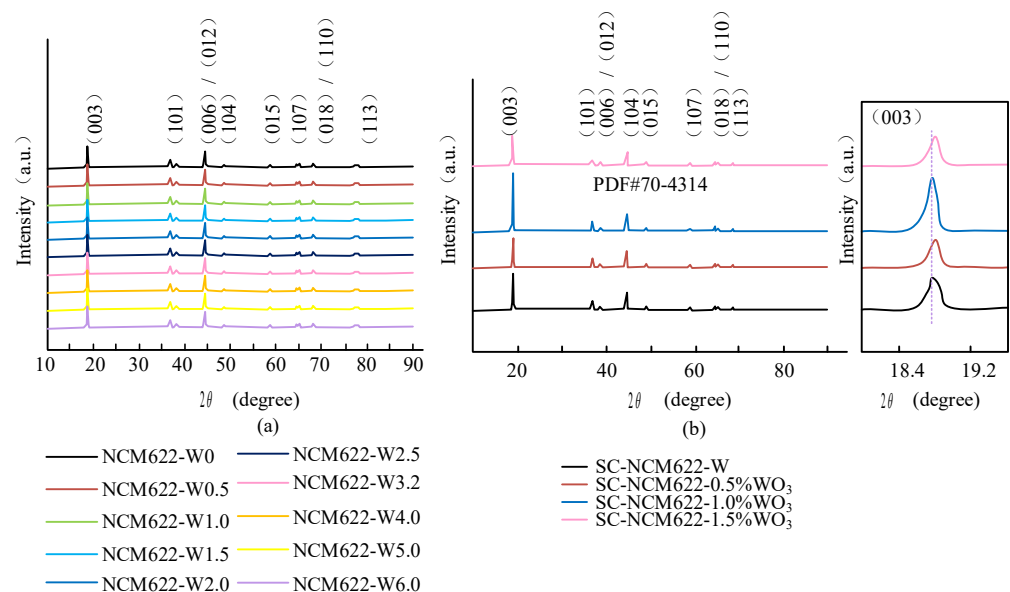

Figure 4. XRD Analysis. (**a**) NCM622-W (**b**) SC-NCM622-W.

Figure 4a displays the effect of WO_3 modification on the phase structure of single-crystal NCM622. Its diffraction peak was consistent with that of PDF card 70-4314, which was typical a-$NaFeO_2$ hexagonal layered structure and belonged to R-3m space group, and no impurities were found. Through diffraction analysis of WO_3, the addition of WO_3 did not change the phase structure of the material, and due to the small amount of WO_3 added, XRD was unable to show the corresponding diffraction peaks of the phase. The two sets of splitting peaks (006)/(102) and (108)/(110) were sharp and clearly split, indicating that the prepared material has a highly ordered layered structure. Figure 4b demonstrates the effect of WO_3 modification on the phase structure of polycrystalline NCM622, presented with the XRD spectra of four samples. The diffraction peaks of the four samples were consistent with the a-$NaFeO_2$ of the space group R-3m, and there was no obvious impurity phase, which means that the addition of WO_3 does not change the phase structure of the polycrystalline material. Meanwhile, due to the small amount of WO_3 added, the corresponding diffraction peak was not detected by XRD. From the local amplification of the (003) diffraction peak, compared to the original sample, the (003) peak of the SC-NCM622-1.0% WO_3 sample shifted significantly towards a lower angle, indicating an increase in the c-axis of the sample. The increased interlayer spacing was significantly beneficial for lithium electron transport during the charging and discharging of the lithium battery [30]. The lattice parameters of the ratio of all samples *I* (003)/*I* (104) are shown in Table 3.

Table 3. The XRD lattice parameters for each sample.

Samples	$a(A)$	$c(A)$	c/a	$V(A)$	*I* (003)/*I* (104)
NCM622-W0	2.868	14.215	4.9564	101.25	1.31
NCM622-W0.5	2.870	14.214	4.9526	101.33	1.27
NCM622-W1.0	2.871	14.221	4.9533	101.50	1.35
NCM622-W1.5	2.870	14.215	4.9530	101.37	1.08
NCM622-W2.0	2.869	14.214	4.9543	101.31	1.17
NCM622-W2.5	2.870	14.213	4.9523	101.38	1.52
NCM622-W3.2	2 870	14. 220	4.9547	101.43	1.23
NCM622-W4.0	2.872	14. 227	4.9537	101.65	1.22
NCM622-W5.0	2.870	14. 222	4.9554	101.40	1.26
NCM622-W6.0	2.875	14.232	4.9503	101.89	1.05
SC-NCM622	2.868	14.213	4.9557	101.264	1.24
SC-NCM622-0.5%WO_3	2.872	14.224	4.9526	101.590	1.07
SC-NCM622-1.0%WO_3	2.868	14.211	4.9550	101.259	1.69
SC-NCM622-1.5%WO_3	2.872	14.221	4.9516	101.565	1.00

Note: If the c/a value is greater than 4.9, it indicates that the crystallinity and development of the sample are good. Generally speaking, if the ratio of *I* (003)/*I* (104) is greater than 12, the degree of cation mixing in the material is lower.

In Table 3, the c/a value represents the layered structure of the sample. From Table 3, with the increase of WO_3 addition, the c/a values of all NCM622-WO_3 samples were greater than 4.95, indicating that the samples before and after WO_3 modification maintained a good layered structure. Compared to the original sample, the lattice constants a and c and the cell volume of the sample modified with WO_3 have increased, indicating that the W element has infiltrated into the lattice structure of the sample. At the same time, the increase in WO_3 will make the sample have higher capacity and better chemical properties. For SC-NCM622 modified with WO_3, Table 3 demonstrates that the *I* (003)/*I* (104) ratio of SC-NCM622-1.0% WO_3 sample was 1.69, which was the highest among all samples. This indicates that adding WO_3 can effectively inhibit the cation mixing of SC-NCM622. Compared to the original sample SC-NCM622, the *I* (003)/*I* (104) values of SC-NCM622-0.5% WO_3 and SC-NCM622-1.5% WO_3 samples have decreased, which may be due to the presence of more Ni^{2+} in the lithium ion layer as the amount of WO_3 added increases. After adding WO_3 at the same time, the peak intensity of the (003) and (104) diffraction peaks in the sample increased, indicating that WO_3 is beneficial for the crystallinity of the ternary material. Overall, although there was a certain difference between a, c, and cell volume in

all samples, the values were small, further proving that the crystal structure of SC-NCM622 was good and has not been destroyed by WO_3 [31]. To observe the morphology and microstructure characteristics of the sample, the SC-NCM622 samples were then subjected to high-resolution TEM versus FFT analysis, as shown in Figure 5.
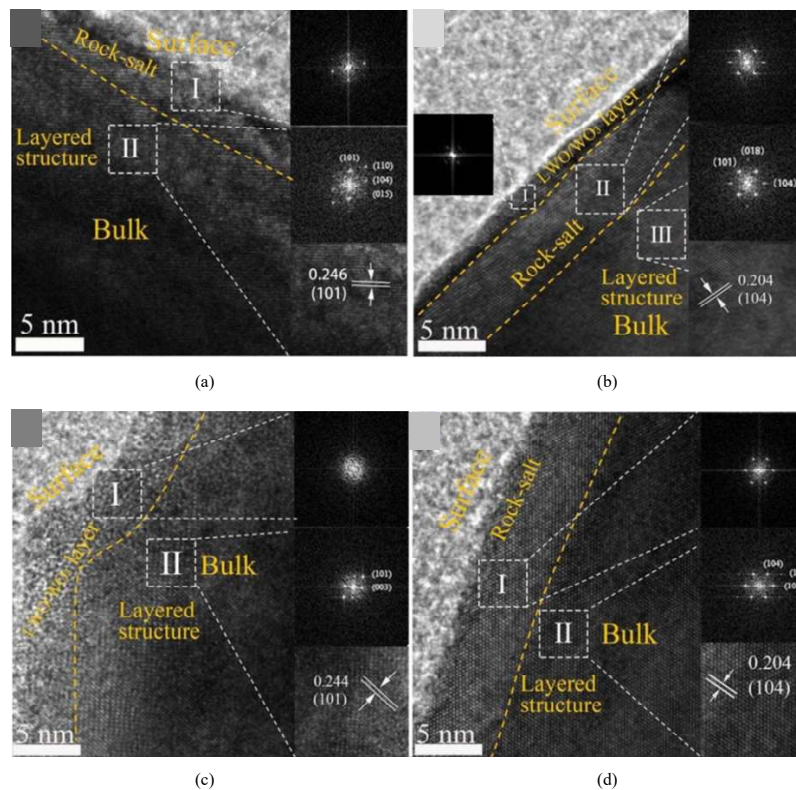

Figure 5. HRTEM map and Fourier transform plots. (**a**) SC-NCM622; (**b**) SC-NCM622-0.5%WO_3; (**c**) SC-NCM622-1.0%WO_3; (**d**) SC-NCM622-1.5%WO_3.

It can be seen from Figure 5 that the outermost layer of the original sample SC-NCM622 has a layer of rock salt facies with a thickness of about 5 nm, and the corresponding space group is Fm-3m, which is mainly due to the mixed discharge of cations. The rock salt phase layer inwards is an ordered layered structure with a space group of R-3m, and the spacing of lattice stripes is 0.246 nm, corresponding to the (101) crystal plane. Compared to the original sample SC-NCM622, the SC-NCM622-0.5% WO_3 sample has an additional LWO/WO_3 coating layer on the outermost layer, with a thickness of approximately 1–2 nm. As a protective layer, the coating can isolate the direct contact between the electrolyte and the active material, reduce the side reaction, and thus improve the electrochemical stability. Moreover, the coating layer can alleviate the structural collapse caused by volume changes caused by lithium removal/insertion during the charging and discharging process of the active material and improve the stability of the layered structure. The coating layer is further divided into rock salt phase and layered phase layer. The thickness of the rock salt phase is thicker compared to the original sample, which is consistent with the XRD refinement results showing that it has a greater cation mixing. In a layered phase, the spacing between atomic layers is 0.204 nm, corresponding to the (104) crystal plane. The HRTEM results indicate that after WO_3 modification, the original structure and crystallinity inside the sample remain intact except for the surface layer. The outermost layer of the SC-NCM622-1.0% WO_3 sample is an LWO/WO_3 layer with a thickness of approximately 5 nm, and the interior is directly a layered phase. The lattice stripe spacing is 0.244 nm, corresponding to the (101) crystal plane. The disappearance of the rock salt phase in this sample indicates that it does not exhibit cation mixing but rather exhibits the characteristics of a lithium rich material, which is consistent with the refined XRD results. The outermost

layer of the SC-NCM622-1.5% WO$_3$ sample is directly the rock salt phase, and the thickness of the rock salt phase is the thickest among all samples, greater than 5 nm, which is caused by the highest degree of cation mixing in the sample, gradually transitioning inward to the layered phase, with a plane spacing of 0.204 nm between the atomic layers of the layered phase, corresponding to the (104) crystal plane. It should be noted that this study cannot distinguish whether the coating layer LWO/WO$_3$ is LWO or WO$_3$ or both. Because in the second stage of calcination after mixing WO$_3$ with the ternary material, WO$_3$ will react with the residual LiOH on the surface of the ternary material to generate LWO compounds. Scanning electron microscopy and EDS analysis were performed on the NCM622-W sample, as expressed in Figure 6.
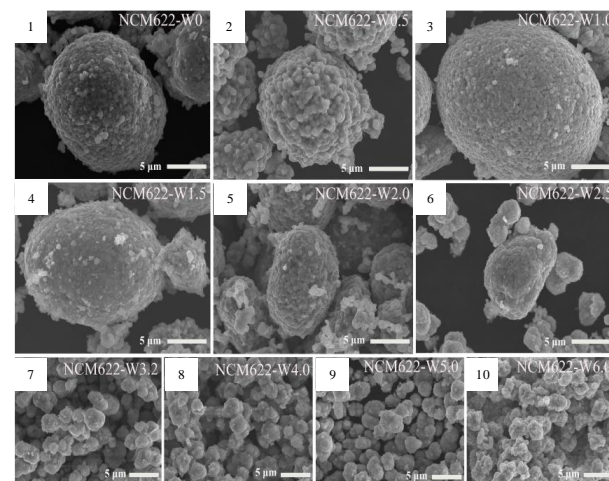
(a)
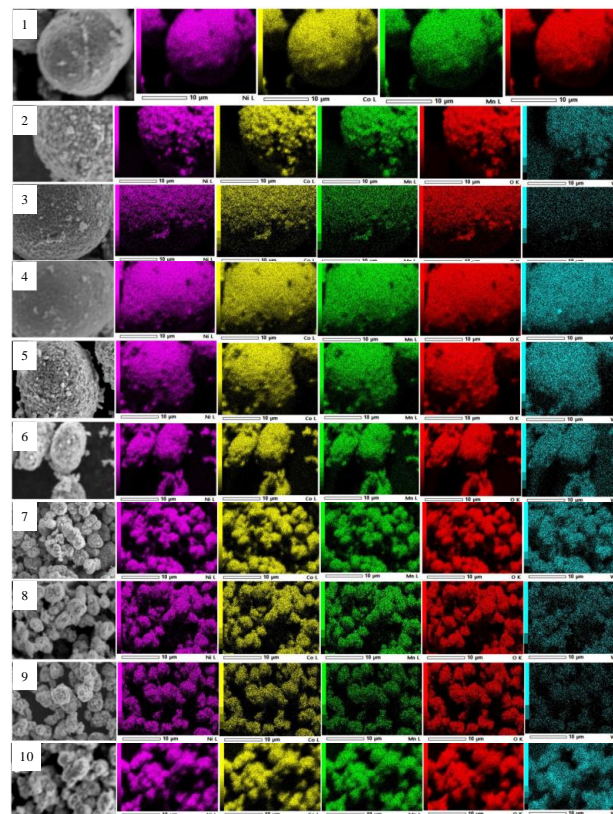
(b)

Figure 6. SEM analysis and EDS element plots. (**a**) SEM analysis; (**b**) EDS Element mapping.

In Figure 6a, with the increase of WO_3 addition, the morphology of all samples changed. When the amount of WO_3 added was small, the NCM622-W sample had good sphericity, and the secondary particle size of the sample was relatively large, reaching 8–10. This indicates that the addition of WO_3 did not alter the morphology of the secondary particles. When the amount of WO_3 added was high, the morphology of NCM622-W sample began to change from spherical to quasi-spherical with a decreasing particle diameter, which was about 4 or smaller. When the amount of WO_3 added was small, the particle surface of NCM622-W sample changed from rough to tight smooth to rough as the amount of WO_3 increases. When the amount of WO_3 added was high, the periodic changes between roughness and smoothness on the surface of the sample particles continue to repeat. The above results denote that the addition of a W element has a significant impact on the crystallization and growth of the material during the calcination. Adding an appropriate amount of WO_3 is beneficial for the surface of particles to become smooth, while adding too much or too little will increase the particle size and make the surface rough. A larger particle size will increase the diffusion path of lithium ions, thereby reducing the RP. Figure 6b shows the EDS test, which shows that the distribution area of the W element and Ni, Co, Mn, and O elements is relatively consistent on the surface of the particle layer, and the surface is uniform [32]. This indicates that WO_3 has been successfully added to the ternary cathode material.

3.2. Analysis of CRP and XPS

The XPS was first tested on each sample, and the test results are shown in Figure 7.
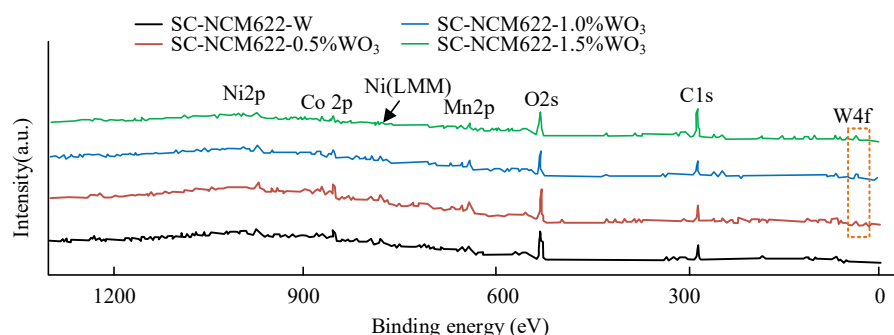

Figure 7. The full spectrum of the SC-NCM622-W sample.

Figure 7 shows the full XPS spectrum, showing the valence states of each element. By comparing the spectra, it was found that all samples exhibited inherent Ni, Co, and Mn characteristic peaks, while the samples added with WO_3 exhibited obvious W element characteristic peaks, indicating that the single-crystal ternary material successfully achieved WO_3 addition. Cyclic and rate performance tests were conducted on each sample in an electrochemical window of 2.8–4.4 V at room temperature [33]. All cycle and rate performance analyses are shown in Figure 8.

Figure 8a shows the magnification performance of all NCM622-W samples. Compared with the original sample NCM622-W0, the magnification performance of the samples after adding WO_3 has been improved to varying degrees, with some of the improvements being very significant. The addition of W increases the migration sites of lithium ions, accelerates the electron conduction speed between particles, improves the conductivity and rate performance of the material, and thus improves the Coulombic efficiency of the electrode battery. At a magnification of 10.0 C, as W increased, the discharge specific capacities of all samples were 124 mAh/g, 37.3 mAh/g, 142 mAh/g, 146.5 mAh/g, 139.5 mAh/g, 143.5 mAh/g, 143.6 mAh/g, 159.5 mAh/g, 136 mAh/g, and 126 mAh/g, respectively. The RP of NCM622-W4.0 sample was particularly outstanding, with a discharge specific capacity ratio of 86.2% at 10.0 C/1.0 C. Moreover, the sample size of NCM622-W4.0 was highly consistent, with regular morphology and smaller particle size. The lithium-ion

transport path was also small, which could significantly improve the diffusion power of lithium ions and ultimately demonstrate superior performance. Therefore, the CP of NCM622-W0 and NCM622-W4.0 samples at high current density 5.0 C magnification was analyzed. In Figure 8b, the CP of the NCM622-W4.0 sample was significantly better than the original one's. After 300 cycles, the discharge specific capacity of NCM622-W4.0 was equivalent to that of the original sample after 200 cycles. This indicates that the addition of W effectively suppresses structural cracking or collapse during the cycling, resulting in excellent CP [34].
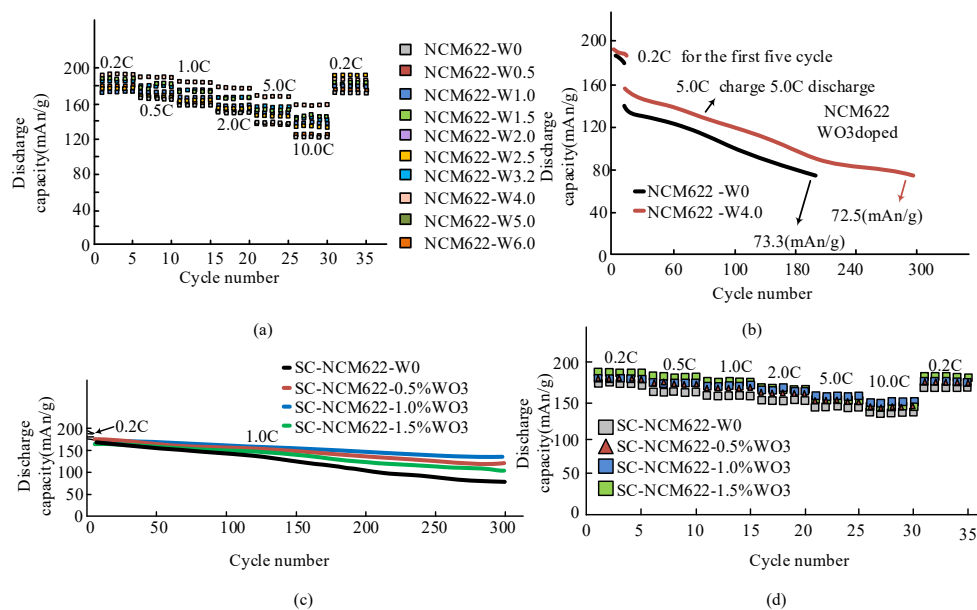

Figure 8. CRP results for all NCM622-W versus SC-NCM622-W samples. (**a**) Multiplication performance of all NCM622-W samples; (**b**) Cyclic performance of NCM622-W0 and NCM622-W4.0 at 5.0C; (**c**) Cyclic performance of all SC-NCM622-W samples; (**d**) Multiplication performance of all SC-NCM622-W samples.

Figure 8c shows the CP of all SC-NCM622-W samples. The first discharge capacity of SC-NCM622 sample at 0.2 C were 190.3 mAh/g, 181.4 mAh/g, 187.2 mAh/g, and 182.5 mAh/g, respectively. The initial capacity of the sample with WO_3 addition had a little difference. After 50 cycles at 1.0 C, the cycle performance curves of all samples remained stable, and the cycle retention rates were 93.4%, 96.1%, 97.5%, and 96.7%, respectively, indicating that the electrochemical process of the samples was highly reversible after the addition of WO_3. After cycling to 300 cycles at 1.0 C, the specific capacity and capacity retention of all samples were improved compared to the original sample SC-NCM622. Taking SC-NCM622-1.0% WO_3 as an example, after long cycles, the discharge specific capacity was 131.5 mAh/g, significantly increasing by 54.8 mAh/g; The capacity retention rate was 76.2%, a significant increase of 31.2%. In summary, the addition of W is a benefit to the formation of a thicker coating layer on the surface of lithium battery samples, reducing the contact area between the active material and the electrolyte, reducing the occurrence of battery side reactions, and effectively alleviating cracks in the sample during charging and discharging, maintaining structural integrity, and significantly improving the CP of SC-NCM622 samples [35].

Figure 8d shows the RP of all SC-NCM622-W samples. The first cycle discharge specific capacities of all samples at 0.2 C were 175.9 mAh/g, 184.3 mAh/g, 182.9 mAh/g, and 190.2 mAh/g, respectively. The specific discharge capacity at 10.0 C magnification were 135.5 mAh/g, 143.5 mAh/g, 148 mAh/g, and 140.5 mAh/g, respectively. By comparison, the discharge specific capacity of the samples significantly increased after the addition of W. Taking the SC-NCM622-1.0% WO_3 sample as an example, the discharge specific capacity at

10.0 C/1.0 C was 86.4%, demonstrating excellent RP. Based on Figure 6, the addition of W has a positive effect on the CRP of lithium batteries, regardless of whether they are doped or coated.

3.3. Cyclic Voltammetry Analysis

The cyclic voltammetry performance of all samples was analyzed under a voltage range of 2.5–4.5 V. The cyclic voltammetry curve is shown in Figure 9.
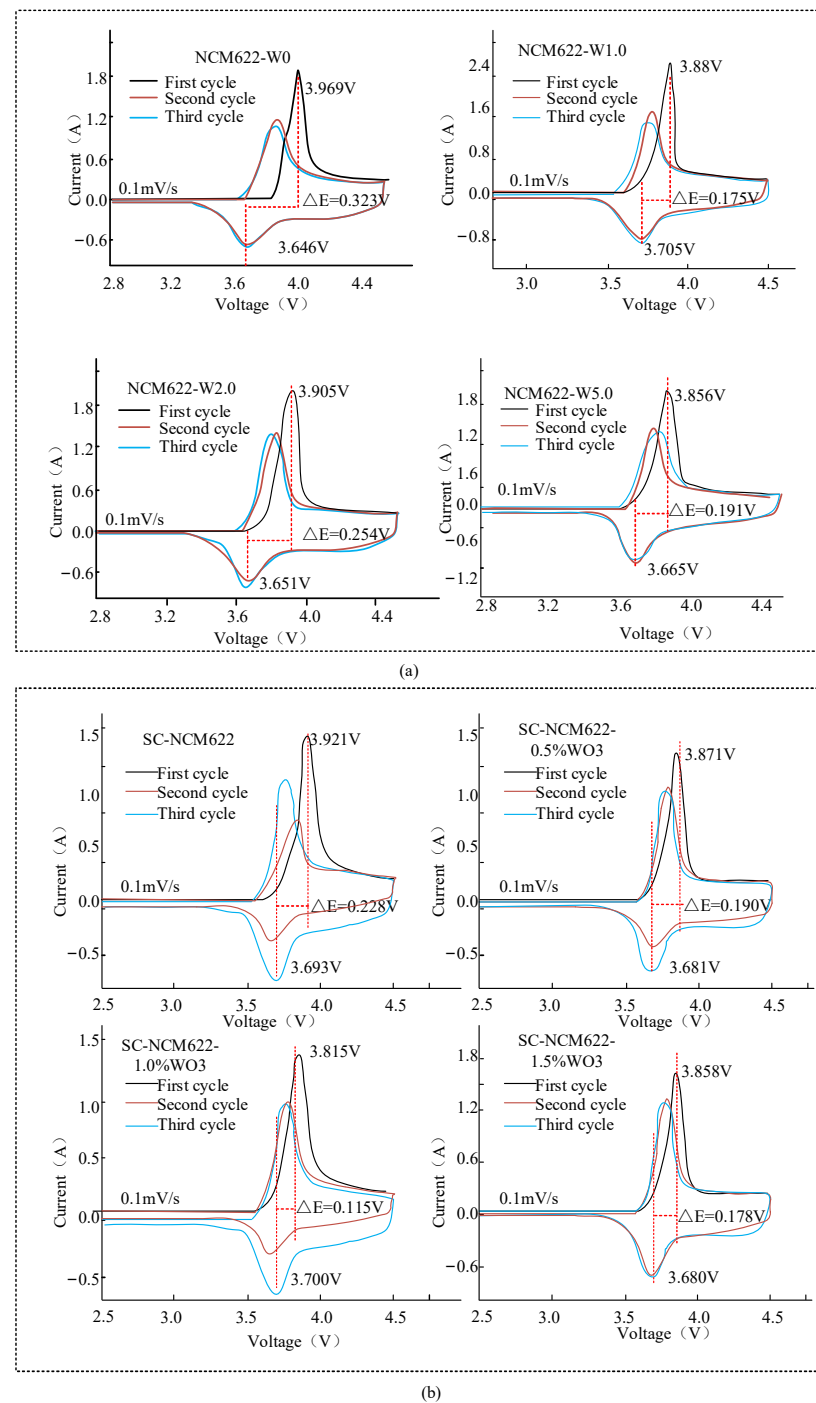

Figure 9. Cyclic voltammetry curve. (**a**) Cyclic Voltammetry Curve of NCM622 Sample; (**b**) Cyclic Voltammetry Curve of SC-NCM622 Sample.

Figure 9a shows the cyclic voltammetry curve of the NCM622 sample. Each sample had a relatively similar cyclic voltammetry curve. Taking NCM622-W0, NCM622-W1.0, NCM622-W2.0, and NCM622-W5.0 as examples, the corresponding potential differences were 0.323 V, 0.175 V, 0.254 V, and 0.191 V, respectively. In contrast with the original sample NCM622-W0, the redox peak potential difference of the sample modified with WO_3 showed a significant decrease. This indicates that WO_3 modification can reduce the polarization phenomenon of ternary cathode materials, thereby slowing down structural degradation and improving the CP of the material. Among them, the oxidation-reduction peak potential difference between NCM622-W1.0 and NCM622-W5.0 samples was the smallest, indicating that the reversibility and stability of lithium ions during the removal and insertion process were higher, the electrode dynamics were faster, the irreversible capacity loss was smaller, and the final cycle stability performance was higher [36]. Figure 9b shows the cycling voltammetry curve of SC-NCM622 sample. The appearance of paired redox peaks represented the redox reaction between Ni^{2+} and Ni^{4+} or Ni^{2+} and Ni^{3+}. As the amount of W increased, the oxidation peaks of the sample were 3.921 V, 3.871 V, 3.815 V, and 3.858 V, respectively. The reduction peaks were 3.693 V, 3.681 V, 3.700 V, and 3.680 V, respectively, and the differences between the redox peaks were 0.228 V, 0.190 V, 0.115 V, and 0.178 V, respectively. This indicates that the addition of WO_3 causes the material to be doped or coated, which is beneficial for reducing the polarization phenomenon of the ternary material, consistent with the results in Figure 9a. When the addition amount of WO_3 was 1.0%, the polarization degree of SC-NCM622 sample was the weakest, indicating that the electrochemical reaction rate of the sample can be faster during the charging and discharging, and the lithium battery can be easily removed and embedded in the electrode, resulting in the optimal EP of the battery.

Figure 10a is the comparison of different cyclic voltammetry curves for NCM622-W1.0, NCM622-W5.0, and the original sample NCM622-W0 with lower polarization. From the figure, the redox peak intensities of NCM622-W1.0 and NCM622-W5.0 were greater than the original sample on the second cyclic voltammetry curve. When cycling 300 times, NCM622-W0 reached 0.522 V; NCM622-W10 reached 0.339 V, and NCM622-W5.0 reached 0.450 V. This indicates that after a long cycle, the original sample will exhibit greater polarization and irreversible capacity loss [37]. At the same time, it was verified that WO_3 modification had a significant good impact on the cyclic stability of the material, which was consistent with the above results. Figure 10b shows the cyclic voltammetry curve of the SC-NCM622 sample battery after 10 cycles at 10 C magnification. From the figure that with the increase of W addition, the redox peak potential differences of each sample after 10 cycles were 0.158 V, 0.097 V, 0.097 V, and 0.132 V, respectively. This indicates that the doping and coating of WO_3 are beneficial for promoting the electrochemical properties of the positive electrode material and avoiding the polarization phenomenon. In addition, the sample added with W showed a higher overlap of the cyclic voltammetry curves of the material, indicating an obvious advancement in the cyclic stability of the material, which conforms to the cyclic performance of the aforementioned material.

3.4. Alternating Current (AC) Impedance Analysis

It analyzes the AC impedance performance of all samples under the same 1.0 C magnification, and the EIS curve is shown in Figure 11.

Figure 11a shows the EIS and equivalent circuit diagrams of NCM622-W samples after six cycles at a magnification of 1.0 C. As shown in the figure, each sample consisted of two semicircles and a diagonal line. Among them, the intersection point of the first semicircle and the x-axis corresponded to Rs in the equivalent circuit diagram, which was the ohmic resistance in the circuit. Rf was the interface impedance of the solid electrolyte; Ret was the charge transfer resistance. The diagonal line represented the Warburg impedance related to material transfer. Figure 11b shows the Nyquist curve and equivalent circuit diagram of all SC-NCM622-W samples charged to 4.4 V after 10 cycles at 1.0 current density. The Nyquist curve consisted of two semicircles in the high and intermediate frequency regions,

as well as a diagonal line in the low-frequency region. In the high-frequency region, Rf was represented as a solid electrolyte thin film resistor. In the mid-frequency range, Ret was the charge transfer impedance. In the low-frequency region, the slope of a straight line was the Warburg impedance related to material transfer [38]. Based on the equivalent circuit diagram, the EIS of each sample were fitted using ZView software. The fitting parameters are presented in Table 4.
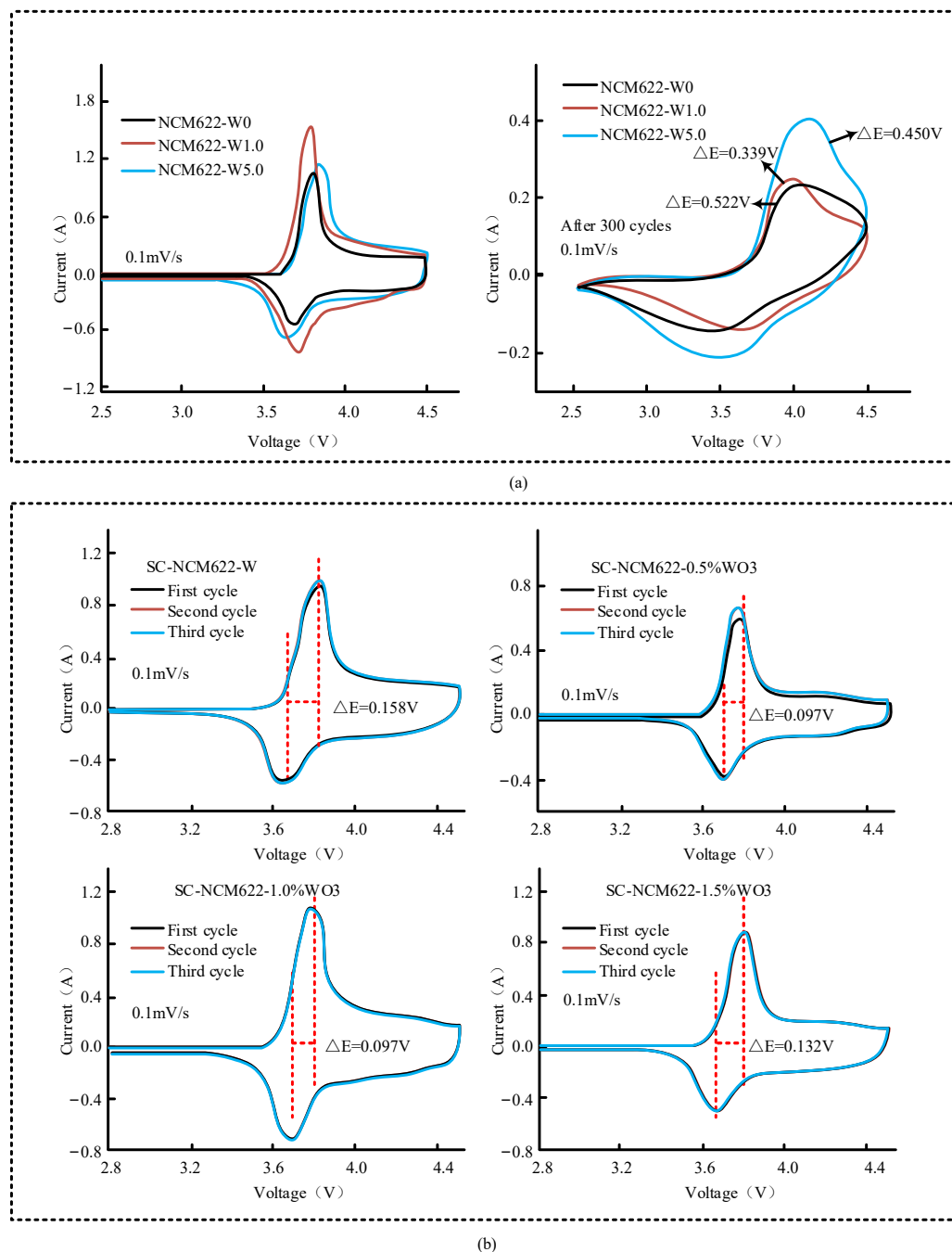

(a)

(b)

Figure 10. Cyclic voltammetry curves at different cycle numbers of the sample. (**a**) Voltammetry curve of NCM622-W with different cycle numbers; (**b**) Cyclic voltammetry curve of SC-NCM622 sample battery after 10 cycles at 10 C magnification.
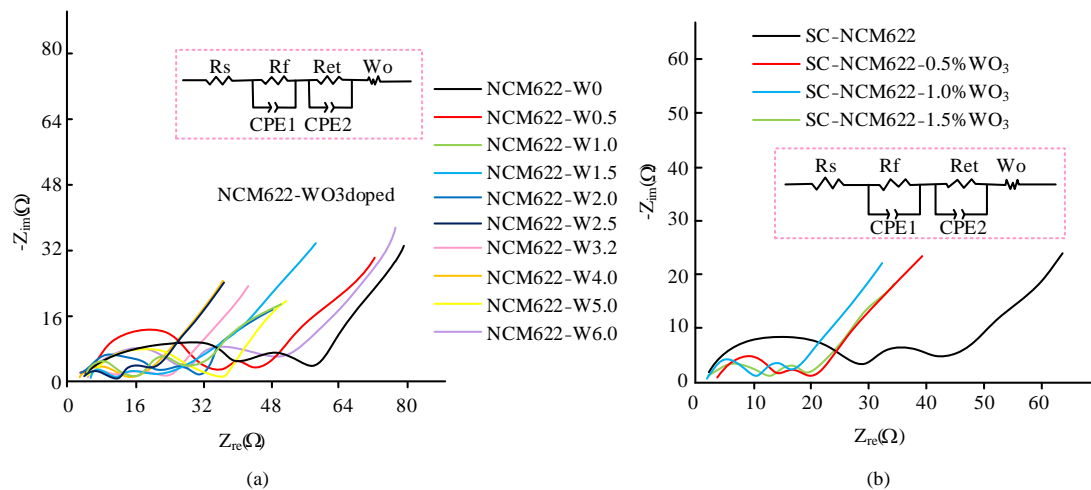
Figure 11. Electrochemical impedance spectroscopy (EIS) test curve of the sample. (**a**) EIS of NCM622W samples after 6 cycles at a magnification of 1.0 C; (**b**) EIS of SC−NCM622−W samples after 10 cycles at 1.0 C.

Table 4. Impedance parameters obtained after fitting the NCM622-W and SC-NCM622-W samples at 1.0 C-Fold cycles.

Samples	Cycles	Rs (Ω)	Rf (Ω)	Rct (Ω)	Rf + Rct (Ω)	$D_{Li}{}^{+}$ (cm^2/s)
NCM622-W0	6th	10.15	13.37	32.1	45.47	3.92×10^{-14}
NCM622-W0.5	6th	4.728	8.13	29.35	37.48	3.21×10^{-14}
NCM622-W1.0	6th	3.724	11.17	11.63	22.80	4.75×10^{-14}
NCM622-W1.5	6th	3.967	15.53	9.989	25.52	2.99×10^{-14}
NCM622-W20.	6th	2.696	18.58	9.007	27.59	4.95×10^{-14}
NCM622-W25	6th	2.99	7761	8.378	16.14	7.64×10^{-14}
NCM622-W3.2	6th	11.13	8795	3.943	12.74	7.59×10^{-14}
NCM622-W4.0.	6th	2.786	9721	5.635	15.36	8.02×10^{-14}
NCM622-W50	6th	5.156	24.71	6.085	30.79	8.40×10^{-14}
NCM622-W6.0	6th	3.837	22.09	12.92	35.01	3.38×10^{-14}
Samples	**Cycles**	**Rs (Ω)**	**Rf (Ω)**	**Rct (Ω)**	**-**	**-**
SC-NCM622	10th	2.097	24.13	15.01	-	-
SC-NCM622-0.5%WO$_3$	10th	3.497	10.23	6.087	-	-
SC-NCM622-1.0%WO$_3$	10th	1.887	8.207	5.849	-	-
SC-NCM622-1.5%WO$_3$	10th	2.102	10.48	6.359	-	-

According to Table 4, after six cycles, compared with the original sample, the Ret and R+Rct values of the NCM622-W sample modified with WO$_3$ showed a significant downward trend. Although the doping of W can aggravate the mixing of lithium ion, Ni^{2+} does not hinder the migration and transport of that. In addition, the expansion of crystal plane spacing caused by doping is beneficial for electron transfer and lithium-ion transport, slowing down the increase in impedance after cycling, delaying the rate of capacity decay, and thereby improving CRP. For the original sample NCM622-W0, due to the influence of the interface between the active substance and the electrolyte, the thickness of the solid electrolyte film significantly increased, resulting in high impedance. At 4.4 V high cutoff voltage, the lithium-ion material battery was extremely unstable in the liquid electrolyte, which makes the structure easy to deteriorate, thus affecting the charge transfer and lithium-ion migration of impedance materials and reducing the EP of materials. According to the data, the lithium-ion transfer coefficient of most material samples has been improved compared to the original sample. Among them, WO$_3$ modification could not only stabilize the main electrode structure but also suppressed the increase in negative

electrode impedance. At the same time, it could accelerate the diffusion of lithium ions on the surface of the positive electrode material, thus improving the EP of the cathode electrode material.

After 10 cycles, compared with the original sample, the Rs and Rf values of the SC-NCM622-W sample modified with WO_3 significantly decreased, indicating a decrease in the internal Ohmic resistance of the obtained sample. At the same time, the doping and coating of W could reduce the bad effects between the electrolyte and the electrode surface and slow down the growth rate of the solid electrolyte film. The addition of W also reduced the Ret value, indicating that WO_3 modification helps promote charge transfer during cycling.

According to calculations, the lithium-ion diffusion coefficients D_{Li}^+ of SC-NCM622, SC-NCM622-0.5% WO_3, SC-NCM622-1.0% WO_3, and SC-NCM622-1.5% WO_3 are 1.14×10^{-15} cm^2/s, 1.36×10^{-15} cm^2/s, 2.06×10^{-15} cm^2/s, and 2.37×10^{-15} cm^2/s, respectively. It can be observed that with the increase of W addition, the diffusion coefficient of lithium ions also significantly increases, resulting in better electrochemical performance. Overall, it can be seen that the kinetic activity of the obtained sample is the best when the addition amount of WO_3 is 1.0%.

4. Conclusions

NRTCMs are highly promising cathode materials for LIB. It studied the modification of poly-crystal and single-crystal nickel-rich ternary material NCM622 using high valent metal compound WO_3 and analyzed the modification effect from four aspects: morphology and structure, cycling and rate, cyclic voltammetry, and AC impedance. It was proved that for SC-NCM622 modified with WO_3, the I (003)/I (104) ratio of SC-NCM622-1.0% WO_3 sample was 1.69, which was the highest among all samples. When the amount of WO_3 added was small, the NCM622-W sample had good sphericity, and the secondary particle size of the sample was relatively large, reaching 8–10. The morphology of the secondary particles did not change. At a magnification of 10.0 C, as W increased, the discharge specific capacities of all samples were 124 mAh/g, 37.3 mAh/g, 142 mAh/g, 146.5 mAh/g, 139.5 mAh/g, 143.5 mAh/g, 143.6 mAh/g, 159.5 mAh/g, 136 mAh/g, and 126 mAh/g, respectively. After 50 cycles at 1.0 C, the cycle performance curves of all samples remained stable, and the cycle retention rates were 93.4%, 96.1%, 97.5%, and 96.7%, respectively, indicating that the electrochemical process of the samples was highly reversible after the addition of WO_3. After cycling to 300 cycles at 1.0 C, the specific capacity and capacity retention of all samples were improved compared to the original sample SC-NCM622. According to calculations, the LIDC D_{Li}^+ of all SC-NCM622-W were 1.14×10^{-15} cm^2/s, 1.36×10^{-15} cm^2/s, 2.06×10^{-15} cm^2/s, and 2.37×10^{-15} cm^2/s, respectively. The modification of WO_3 resulted in changes in the particle morphology of the material, enhanced cycling stability and RP of the battery, and significantly improved EP of the electrode material. However, the size of the prepared single-crystal particles was small, and there were fine particles attached, so the structural collapse was still serious. Therefore, it is necessary to continue to improve the synthesis and obtain a single crystal with a large and uniform particle size to further optimize the modification effect.

Conflicts of Interest: The authors declare no conflict of interest.

References

1. Fu, F.; Liu, X.; Fu, X.; Chen, H.; Huang, L.; Fan, J.; Le, J.; Wang, Q.; Yang, W.; Ren, Y.; et al. Entropy and crystal-facet modulation of P2-type layered cathodes for long-lasting sodium-based batteries. *Nat. Commun.* **2022**, *13*, 2826. [CrossRef] [PubMed]
2. Vasko, F.J.; Lu, Y.; McNally, B. A Simple Methodology that Efficiently Generates All Optimal Spanning Trees for the Ca-ble-Trench Problem. *J. Comput. Cogn. Eng.* **2022**, *1*, 13–20.
3. Sarkar, A.; Biswas, A.; Kundu, M. Development of q-Rung Orthopair Trapezoidal Fuzzy Einstein Aggregation Operators and Their Application in MCGDM Problems. *J. Comput. Cogn. Eng.* **2022**, *1*, 109–121.
4. Mu, K.; Cao, Y.; Hu, G.; Du, K.; Yang, H.; Gan, Z.; Peng, Z. Enhanced electrochemical per-formance of Li-rich cathode $Li_{1.2}Ni_{0.2}Mn_{0.6}O_2$ by surface modification with WO_3 for lithium ion batteries. *Electrochim. Acta* **2018**, *273*, 88–97. [CrossRef]
5. Gholami, P.; Khataee, A.; Bhatnagar, A.; Vahid, B. Synthesis of N-doped magnetic WO_3–x@ Mesoporous carbon using a diatom template and plasma modification: Visible-light-Driven Photocatalytic activities. *ACS Appl. Mater. Interfaces* **2021**, *13*, 13072–13086. [CrossRef]
6. Das, K.K.; Sahoo, D.; Mansingh, S.; Parida, K. $ZnFe_2O_4@WO_3$-X/Polypyrrole: An Efficient Ternary Photocatalytic System for Energy and Environmental Application. *ACS Omega* **2021**, *6*, 30401–30418.
7. Wang, B.; Zhang, F.-L.; Zhou, X.-A.; Wang, P.; Wang, J.; Ding, H.; Dong, H.; Liang, W.-B.; Zhang, N.-S.; Li, S.-Y. Which of the nickel-rich NCM and NCA is structurally superior as a cathode material for lithium-ion batteries? *J. Mater. Chem. A* **2021**, *9*, 13540–13551. [CrossRef]
8. Xiao, Z.; Liu, P.; Song, L.; Cao, Z.; Du, J.; Zhou, C. The correlation between structure and thermal properties of nickel-rich ternary cathode materials: A review. *Ionics* **2021**, *27*, 3207–3217. [CrossRef]
9. Lee, G.; Jung, K.; Lee, Y.; Kim, J.; Yim, T. Interface-Stabilized Layered Lithium Ni-Rich Oxide Cathode via Surface Functionali-zation with Titanium Silicate. *ACS Appl. Mater. Interfaces* **2021**, *13*, 47696–47705. [CrossRef]
10. Mao, G.; Luo, J.; Zhou, Q.; Xiao, F.; Tang, R.; Li, J. Improved cycling stability of high nickel cathode material for lithium ion battery through Al- and Ti-based dual modification. *Nanoscale* **2021**, *44*, 18741–18753. [CrossRef] [PubMed]
11. Xia, D.; Hu, S.; Ding, N.; Wen, M.; Xiao, Q.; Zhong, S. Submicron single-crystal structure for enhanced structural stability of LiNi0.8Mn0.2O2 Ni-rich cobalt-free cathode materials. *Ionics* **2023**, *29*, 1699–1709. [CrossRef]
12. Geng, Z.; Shi, W.; Wang, J.; Zhang, X.; Hu, N.; Wang, S. A high-voltage solid-state organic lithium battery based on 2,3,5,6-tetrafluoro-7,7,8,8-tetracyanoquinodimethane cathode. *Int. J. Energy Res.* **2022**, *9*, 12316–12322. [CrossRef]
13. Kaneda, H.; Furuichi, Y.; Ikezawa, A.; Arai, H. Effects of aluminum substitution in nickel-rich layered $LiNixAl1xO_2$ (x = 0.92, 0.95) positive electrode materials for Li-ion batteries on high-rate cycle performance. *J. Mater. Chem. A* **2021**, *38*, 21981–21994. [CrossRef]
14. Xiao, C.; Xia, M.; Ye, W.; Zhang, X.; Chen, S.; Yu, H.; Bi, W.; Shui, M.; Shu, J. The positive effect of nitridation on $CrNb_{49}O_{124}$ nanowires for high-performance lithium-ion storage. *Ceram. Int.* **2020**, *46*, 15527–15533. [CrossRef]
15. Fang, W.; Lin, Y.; Xv, R.; Fu, L. Boosting Photoelectrochemical Performance of $BiVO_4$ Photoanode by Synergistic Effect of WO_3/$BiVO_4$ Heterojunction Construction and NiOOH Water Oxidation Cocatalyst Modification. *ACS Appl. Energy Mater.* **2022**, *5*, 11402–11412. [CrossRef]
16. Li, X.; Ai, M.; Zhang, X.; Zou, J.J.; Pan, L. Dual co-catalysts decorated Zn-WO_3 nanorod arrays with highly efficient photoelec-trocatalytic performance. *Int. J. Hydrogen Energy* **2022**, *47*, 13641–13653. [CrossRef]
17. Ou, L.; Nong, S.; Yang, R.; Li, Y.; Tao, J.; Zhang, P.; Zhou, W. Multi-Role Surface Modification of Single-Crystalline Nickel-Rich Lithium Nickel Cobalt Manganese Oxides Cathodes with WO_3 to Improve Performance for Lithium-Ion Batteries. *Nanomaterials* **2022**, *12*, 1324. [CrossRef] [PubMed]
18. Yin, X.; Qiu, W.; Li, W.; Wang, K.; Yang, X.; Du, L.; Li, J. Effects of alkali ion on boosting WO_3 photoelectrochemical performance by electrochemical doping. *Int. J. Hydrogen Energy* **2020**, *45*, 19257–19266. [CrossRef]
19. Bekarevich, R.; Pihosh, Y.; Tanaka, Y.; Nishikawa, K.; Matsushita, Y.; Hiroto, T.; Takada, K. Conversion reaction in the bind-er-free anode for fast-charging Li-ion batteries based on WO_3 nanorods. *ACS Appl. Energy Mater.* **2020**, *3*, 6700–6708. [CrossRef]
20. Khan, K.; Fu, B.; Xin, H.; Beshiwork, B.A.; Hanif, M.B.; Wu, J.; Wu, M. Composite polymer electrolyte incorporating WO_3 nanofillers with enhanced performance for dendrite-free solid-state lithium battery. *Ceram. Int.* **2023**, *49*, 4473–4481. [CrossRef]
21. Sun, J.; Li, L.; Ge, S.; Zhao, P.; Zhu, P.; Wang, M.; Yu, J. Dual-mode aptasensor assembled by a WO_3/Fe_2O_3 heterojunction for paper-based colorimetric prediction/photoelectrochemical multicomponent analysis. *ACS Appl. Mater. Interfaces* **2021**, *13*, 3645–3652. [CrossRef]
22. Hu, C.; Li, L.; Zhou, J.; Li, B.; Zhao, S.; Zou, C. Enhanced Contrast of WO_3-Based Smart Windows by Continuous Li-Ion Insertion and Metal Electroplating. *ACS Appl. Mater. Interfaces* **2022**, *14*, 32253–32260. [CrossRef]
23. Tan, X.; Yu, H.; Liang, B.; Han, M.; Ge, S.; Zhang, L.; Yu, J. A target-driven self-feedback paper-based photoelectrochemical sensing platform for ultrasensitive detection of ochratoxin A with an In_2S_3/WO_3 heterojunction structure. *Anal. Chem.* **2022**, *94*, 1705–1712. [CrossRef]
24. Li, Y.; Zhang, W.; Qiu, B. Enhanced surface charge separation induced by Ag nanoparticles on WO_3 photoanode for photoelectro-chemical water splitting. *Chem. Lett.* **2020**, *49*, 741–744. [CrossRef]

25. Long, X.M.; Chen, Y.J.; Zhou, J. Development of AR Experiment on Electric-Thermal Effect by Open Framework with Simulation-Based Asset and User-Defined Input. In *Artificial Intelligence and Applications*; Bon View Publishing: Singapore, 2023; Volume 1, pp. 52–57.
26. Dang, X.; Jiang, X.; Zhang, T.; Zhao, H. WO_3 inversce opal photonic crystals: Unique property, synthetic methods and extensive application. *Chin. J. Chem.* **2021**, *39*, 1706–1715. [CrossRef]
27. Li, T.; Guo, X.; Zhang, L.; Yan, T.; Jin, Z. 2D CoP supported 0D WO_3 constructed S-scheme for efficient photocatalytic hydro-gen evolution. *Int. J. Hydrogen Energy* **2021**, *46*, 20560–20572. [CrossRef]
28. Wang, J.; Shao, Y.; Yuan, F.; Sun, H.; Zhang, D.; Li, Z.; Wang, B. Hierarchically designed $MoWSe_2/WO_3/C$ anode for fast and efficient Na^+ storage. *J. Energy Chem.* **2023**, *80*, 291–301. [CrossRef]
29. Islam, A.; Othman, F.; Sakib, N.; Babu, H.M.H. Prevention of Shoulder-Surfing Attack Using Shifting Condition with the Digraph Substitu-tion Rules. In *Artificial Intelligence and Applications*; Bon View Publishing: Singapore, 2023; Volume 1, pp. 58–68.
30. Lou, F.; Xie, Q.; Luo, X.; Xie, Y.; Wang, M.; Hao, H.; Wang, Z.; Yang, L.; Wang, G.; Chen, J.; et al. Preventing Structural Collapse and Thermal Runaway to Im-prove the Electrochemical Performance and Safety of $LiNi_{0.8}Co_{0.1}Mn_{0.1}O_2$ by a Negative-Thermal-Expansion Material of $Al_2 (WO_3)_4$. *Ind. Eng. Chem. Res.* **2022**, *61*, 4588–4600. [CrossRef]
31. Shenouda, S.S.; Al Abdulaal, T.H.; Zahran, H.Y.; Yahia, I.S. Synthesis, structure identification and linear/nonlinear optics of hy-drothermally grown WO_3 nanostructured thin film/FTO: Novel approach. *Ceram. Int.* **2022**, *48*, 7663–7667. [CrossRef]
32. Samuel, O.; Othman MH, D.; Kamaludin, R.; Sinsamphanh, O.; Abdullah, H.; Puteh, M.H.; Kurniawan, T.A. WO_3–based photo-catalysts: A review on synthesis, performance enhancement and photocatalytic memory for environmental applications. *Ceram. Int.* **2022**, *48*, 5845–5875. [CrossRef]
33. Bingah, O.K.; Pritzker, M.D. Graphite felt modified with WO_3, SnO_2, and binary WO_3/SnO_2-mixtures as novel positive elec-trodes for cerium-based redox flow batteries. *Int. J. Energy Res.* **2022**, *46*, 4680–4698. [CrossRef]
34. Badiezadeh, F.; Kimiagar, S. Modified WO_3 nanosheets by N-GO nanocomposites to form NO_2 sensor. *J. Exp. Nanosci.* **2021**, *16*, 144–158. [CrossRef]
35. Sun, Y.; Ren, D.; Liu, G.; Mu, D.; Wang, L.; Wu, B. Correlation between thermal stabilities of nickel-rich cathode materials and battery thermal runaway. *Int. J. Energy Res.* **2021**, *45*, 20867–20877. [CrossRef]
36. Li, W.; Zhang, J.; Zhou, Y.; Huang, W.; Liu, X.; Li, Z.; Gao, M.; Chang, Z.; Li, N.; Wang, J.; et al. Regulating the Grain Orientation and Surface Structure of Primary Particles through Tungsten Modification to Comprehensively Enhance the Performance of Nickel-Rich Cathode Materials. *ACS Appl. Mater. Interfaces* **2020**, *12*, 47513–47525. [CrossRef] [PubMed]
37. Chen, Z.; Gao, X.; Kim, J.; Kim, G.; Passerini, S. Quasi-Solid-State Lithium Metal Batteries Using the $LiNi_{0.8}Co_{0.1}Mn_{0.1}O_2$-Li1+xAlxTi2-x(PO4)3 Composite Positive Electrode. *ACS Appl. Mater. Interfaces* **2021**, *13*, 53810–53817. [CrossRef] [PubMed]
38. Takeuchi, T.; Kageyama, H.; Nakanishi, K.; Kiuchi, H.; Katayama, M.; Inada, Y. Improvement of Cycle Capability of Fe-Substituted Li_2S-Based Positive Electrode Materials by Doping with Lithium Iodide. *J. Electrochem. Soc.* **2019**, *166*, 5231–5236. [CrossRef]